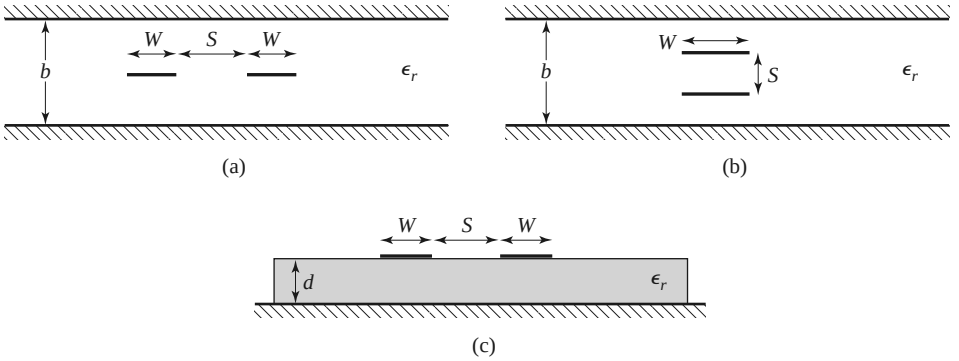

FIGURE 7.26 Various coupled transmission line geometries. (a) Coupled stripline (planar, or edge-coupled). (b) Coupled stripline (stacked, or broadside-coupled). (c) Coupled microstrip lines.

7.6 COUPLED LINE DIRECTIONAL COUPLERS

When two unshielded transmission lines are in close proximity, power can be coupled from one line to the other due to the interaction of the electromagnetic fields. Such lines are referred to as *coupled transmission lines*, and they usually consist of three conductors in close proximity, although more conductors can be used. Figure 7.26 shows several examples of coupled transmission lines. Coupled transmission lines are sometimes assumed to operate in the TEM mode, which is rigorously valid for coaxial line and stripline structures, but only approximately valid for microstrip line, coplanar waveguide, or slotline structures. Coupled transmission lines can support two distinct propagating modes, and this feature can be used to implement a variety of practical directional couplers, hybrids, and filters.

The coupled lines shown in Figure 7.26 are symmetric, meaning that the two conducting strips have the same width and position relative to ground; this simplifies the analysis of their operation. We will first discuss the basic theory of coupled lines and present some design data for coupled stripline and coupled microstrip line. We will then analyze the operation of a single-section coupled line directional coupler and extend these results to multisection coupled line coupler design.

Coupled Line Theory

The coupled lines of Figure 7.26, or other symmetric three-wire lines, can be represented by the structure and equivalent circuit shown in Figure 7.27. If we assume TEM propagation, then the electrical characteristics of the coupled lines can be completely determined from the effective capacitances between the lines and the velocity of propagation on the line. As depicted in Figure 7.27, C_{12} represents the capacitance between the two strip conductors, and C_{11} and C_{22} represent the capacitance between one strip conductor

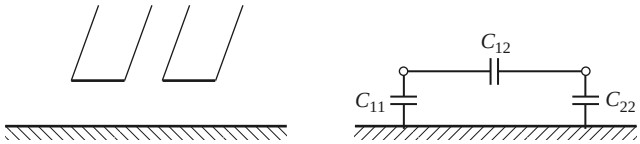

FIGURE 7.27 A three-wire coupled transmission line and its equivalent capacitance network.

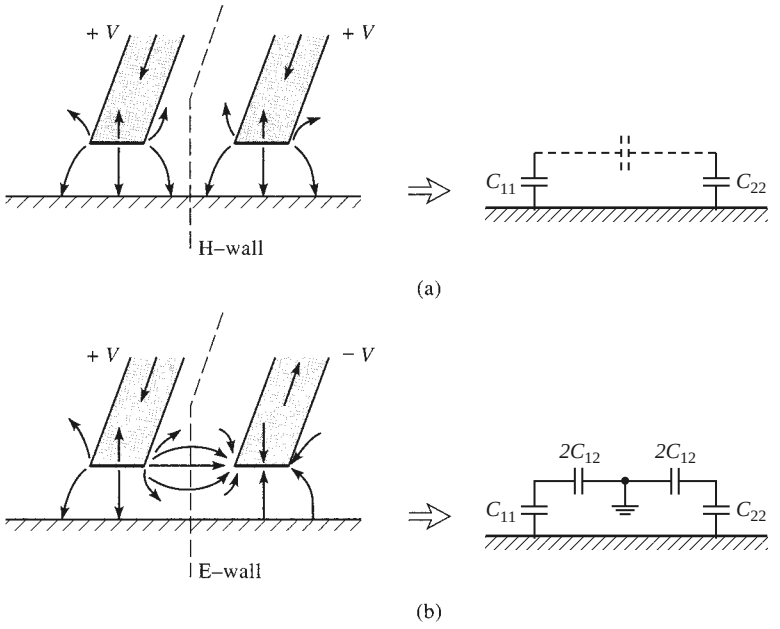

FIGURE 7.28 Even- and odd-mode excitations for a coupled line, and the resulting equivalent capacitance networks. (a) Even-mode excitation. (b) Odd-mode excitation.

and ground. Because the strip conductors are identical in size and location relative to the ground conductor, we have $C_{11} = C_{22}$. Note that the designation of "ground" for the third conductor has no special relevance beyond the fact that it is convenient, since in many applications this conductor is the ground plane of a stripline or microstrip circuit.

Now consider two special types of excitations for the coupled line: the even mode, where the currents in the strip conductors are equal in amplitude and in the same direction, and the odd mode, where the currents in the strip conductors are equal in amplitude but in opposite directions. The electric field lines for these two cases are sketched in Figure 7.28. Because the line is TEM, the propagation constant and phase velocity are the same for both of these modes: $\beta = \omega/v_p$ and $v_p = c/\sqrt{\epsilon_r}$, where ϵ_r is the relative permittivity of the TEM line.

For the even mode, the electric field has even symmetry about the center line, and no current flows between the two strip conductors. This leads to the equivalent circuit shown, where C_{12} is effectively open-circuited. The resulting capacitance of either line to ground for the even mode is

$$C_e = C_{11} = C_{22}, \tag{7.68}$$

assuming that the two strip conductors are identical in size and location. Then the characteristic impedance for the even mode is

$$Z_{0e} = \sqrt{\frac{L_e}{C_e}} = \frac{\sqrt{L_e C_e}}{C_e} = \frac{1}{v_p C_e}, \tag{7.69}$$

where $v_p = c/\sqrt{\epsilon_r} = 1/\sqrt{L_e C_e} = 1/\sqrt{L_o C_o}$ is the phase velocity of propagation on the line.

For the odd mode, the electric field lines have an odd symmetry about the center line, and a voltage null exists between the two strip conductors. We can imagine this as a ground

plane through the middle of C_{12}, which leads to the equivalent circuit shown. In this case the effective capacitance between either strip conductor and ground is

$$C_o = C_{11} + 2C_{12} = C_{22} + 2C_{12}, \tag{7.70}$$

and the characteristic impedance for the odd mode is

$$Z_{0o} = \sqrt{\frac{L_o}{C_o}} = \frac{\sqrt{L_o C_o}}{C_o} = \frac{1}{v_p C_o}. \tag{7.71}$$

In words, Z_{0e} (Z_{0o}) is the characteristic impedance of one of the strip conductors relative to ground when the coupled line is operated in the even (odd) mode. An arbitrary excitation of a coupled line can always be treated as a superposition of appropriate amplitudes of even- and odd-mode excitations. This analysis assumes the lines are symmetric, and that fringing capacitances are identical for even and odd modes.

If the coupled line supports a pure TEM mode, such as coaxial line, parallel plate guide, or stripline, analytical techniques such as conformal mapping [7] can be used to evaluate the capacitances per unit length of line, and the even- and odd-mode characteristic impedances can then be determined. For quasi-TEM lines, such as microstrip line, these results can be obtained numerically or by approximate quasi-static techniques [8]. In either case, such calculations are generally too involved for our consideration, but many commercial microwave CAD packages can provide design data for a variety of coupled lines. Here we will present only graphical design data for two cases of coupled lines.

For a symmetric coupled stripline of the type shown in Figure 7.26a, the design graph in Figure 7.29 can be used to determine the necessary strip widths and spacing for a given set of characteristic impedances, Z_{0e} and Z_{0o}, and the dielectric constant. This graph

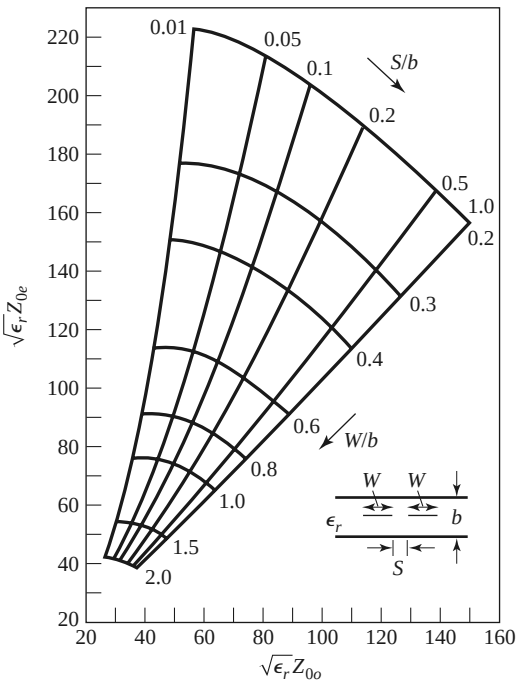

FIGURE 7.29 Normalized even- and odd-mode characteristic impedance design data for symmetric edge-coupled striplines.

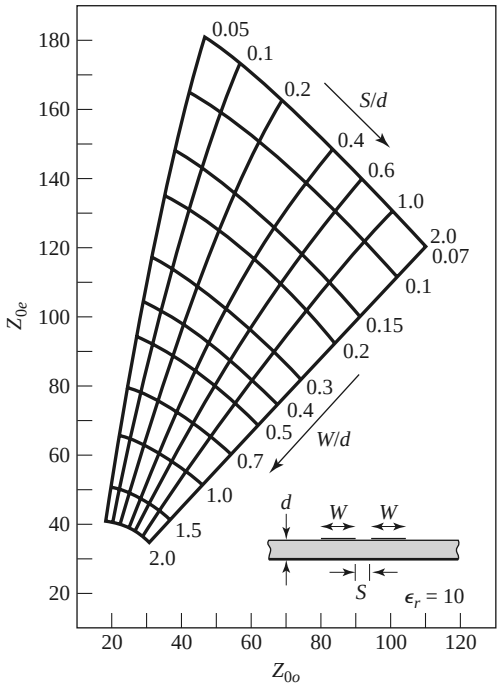

FIGURE 7.30 Even- and odd-mode characteristic impedance design data for symmetric coupled microstrip lines on a substrate with $\epsilon_r = 10$.

should cover ranges of parameters for most practical applications, and can be used for any dielectric constant, since the TEM mode of stripline allows scaling by the dielectric constant.

For coupled microstrip lines, the results do not scale with dielectric constant, so design graphs must be made for specific values of dielectric constant. Figure 7.30 shows such a design graph for symmetric coupled microstrip lines on a substrate with $\epsilon_r = 10$. Another difficulty with coupled microstrip lines is the fact that the phase velocity is usually different for the two modes of propagation because the two modes operate with different field configurations in the vicinity of the air–dielectric interface. This can have a degrading effect on coupler directivity.

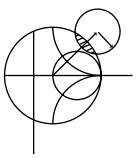

EXAMPLE 7.6 IMPEDANCE OF A SIMPLE COUPLED LINE

For the broadside coupled stripline geometry of Figure 7.26b, assume $W \gg S$ and $W \gg b$, so that fringing fields can be ignored, and determine the even- and odd-mode characteristic impedances.

Solution

We first find the equivalent network capacitances, C_{11} and C_{12} (because the line is symmetric, $C_{22} = C_{11}$). The capacitance per unit length of broadside parallel lines with width W and separation d is

$$\bar{C} = \frac{\epsilon W}{d} \text{ F/m},$$

where ϵ is the substrate permittivity. This formula ignores fringing fields.

C_{11} is formed by the capacitance of one strip to the ground planes. Thus the capacitance per unit length is

$$\bar{C}_{11} = \frac{2\epsilon_r \epsilon_0 W}{b - s} \text{ F/m.}$$

The capacitance per unit length between the strips is

$$\bar{C}_{12} = \frac{\epsilon_r \epsilon_0 W}{S} \text{ F/m.}$$

Then from (7.68) and (7.70), the even- and odd-mode capacitances are

$$\bar{C}_e = \bar{C}_{11} = \frac{2\epsilon_r \epsilon_0 W}{b - S} \text{ F/m,}$$

$$\bar{C}_o = \bar{C}_{11} + 2\bar{C}_{12} = 2\epsilon_r \epsilon_0 W \left(\frac{1}{b - S} + \frac{1}{S} \right) \text{ F/m.}$$

The phase velocity on the line is $v_p = 1/\sqrt{\epsilon_r \epsilon_0 \mu_0} = c/\sqrt{\epsilon_r}$, so the characteristic impedances are

$$Z_{0e} = \frac{1}{v_p \bar{C}_e} = \eta_0 \frac{b - S}{2W\sqrt{\epsilon_r}},$$

$$Z_{0o} = \frac{1}{v_p \bar{C}_o} = \eta_0 \frac{1}{2W\sqrt{\epsilon_r}[1/(b - S) + 1/S]}.$$ ■

Design of Coupled Line Couplers

With the preceding definitions of the even- and odd-mode characteristic impedances, we can apply an even-odd mode analysis to a length of coupled line to arrive at the design equations for a single-section coupled line coupler. Such a line is shown in Figure 7.31. This four-port network is terminated in the impedance Z_0 at three of its ports, and driven with a generator of voltage $2V_0$ and internal impedance Z_0 at port 1. We will show that a coupler can be designed with arbitrary coupling such that the input (port 1) is matched, while port 4 is isolated. Port 2 is the through port, and port 3 is the coupled port. In Figure 7.31, a ground conductor is understood to be common to both strip conductors.

For this problem we will apply the even-odd mode analysis technique in conjunction with the voltages and currents on the line, as opposed to the reflection and transmission coefficients. So, by superposition, the excitation at port 1 in Figure 7.31 can be treated as the sum of the even- and odd-mode excitations shown in Figure 7.32. From symmetry we can see that $I_1^e = I_3^e$, $I_4^e = I_2^e$, $V_1^e = V_3^e$, and $V_4^e = V_2^e$ for the even mode, while $I_1^o = -I_3^o$, $I_4^o = -I_2^o$, $V_1^o = -V_3^o$, and $V_4^o = -V_2^o$ for the odd mode. The input impedance at port 1 of the coupler of Figure 7.31 can then be expressed as

$$Z_{\text{in}} = \frac{V_1}{I_1} = \frac{V_1^e + V_1^o}{I_1^e + I_1^o}. \tag{7.72}$$

If we let Z_{in}^e be the input impedance at port 1 for the even mode, and Z_{in}^o be the input impedance for the odd mode, then we have

$$Z_{\text{in}}^e = Z_{0e} \frac{Z_0 + jZ_{0e} \tan\theta}{Z_{0e} + jZ_0 \tan\theta}, \tag{7.73a}$$

$$Z_{\text{in}}^o = Z_{0o} \frac{Z_0 + jZ_{0o} \tan\theta}{Z_{0o} + jZ_0 \tan\theta}, \tag{7.73b}$$

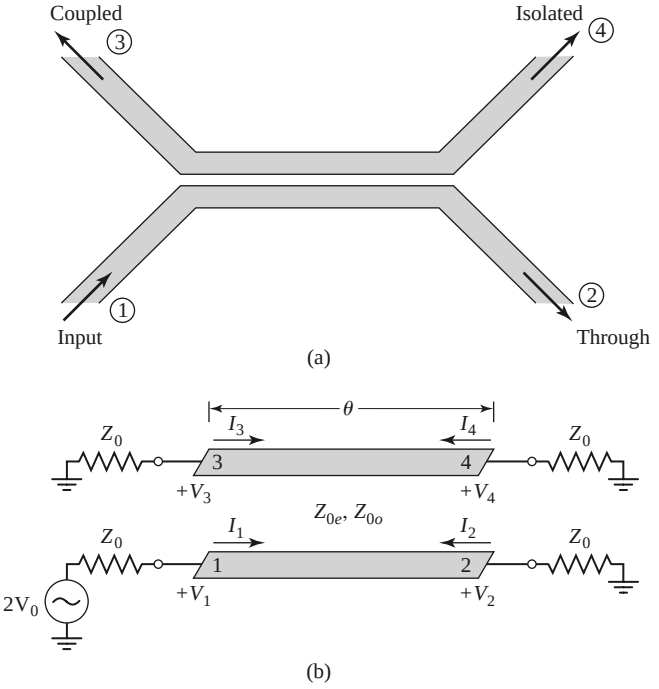

FIGURE 7.31 A single-section coupled line coupler. (a) Geometry and port designations. (b) The schematic circuit.

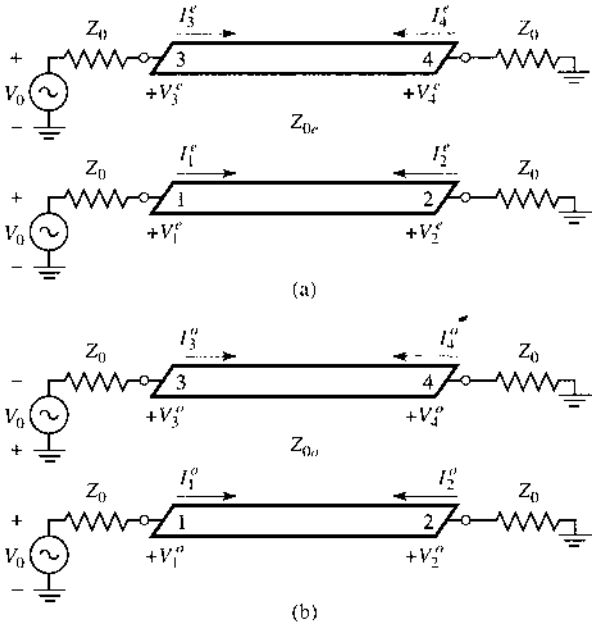

FIGURE 7.32 Decomposition of the coupled line coupler circuit of Figure 7.31 into even- and odd-mode excitations. (a) Even mode. (b) Odd mode.

since, for each mode, the line looks like a transmission line of characteristic impedance Z_{0e} or Z_{0o}, terminated in a load impedance, Z_0. Then by voltage division,

$$V_1^o = V_0 \frac{Z_{\text{in}}^o}{Z_{\text{in}}^o + Z_0}, \tag{7.74a}$$

$$V_1^e = V_0 \frac{Z_{\text{in}}^e}{Z_{\text{in}}^e + Z_0}, \tag{7.74b}$$

and

$$I_1^o = \frac{V_0}{Z_{\text{in}}^o + Z_0}, \tag{7.75a}$$

$$I_1^e = \frac{V_0}{Z_{\text{in}}^e + Z_0}. \tag{7.75b}$$

Using these results in (7.72) yields

$$Z_{\text{in}} = \frac{Z_{\text{in}}^o\left(Z_{\text{in}}^e + Z_0\right) + Z_{\text{in}}^e\left(Z_{\text{in}}^o + Z_0\right)}{Z_{\text{in}}^e + Z_{\text{in}}^o + 2Z_0} = Z_0 + \frac{2\left(Z_{\text{in}}^o Z_{\text{in}}^e - Z_0^2\right)}{Z_{\text{in}}^e + Z_{\text{in}}^o + 2Z_0}. \tag{7.76}$$

Now if we let

$$Z_0 = \sqrt{Z_{0e} Z_{0o}}, \tag{7.77}$$

then (7.73a) and (7.73b) reduce to

$$Z_{\text{in}}^e = Z_{0e} \frac{\sqrt{Z_{0o}} + j\sqrt{Z_{0e}} \tan\theta}{\sqrt{Z_{0e}} + j\sqrt{Z_{0o}} \tan\theta},$$

$$Z_{\text{in}}^o = Z_{0o} \frac{\sqrt{Z_{0e}} + j\sqrt{Z_{0o}} \tan\theta}{\sqrt{Z_{0o}} + j\sqrt{Z_{0e}} \tan\theta},$$

so that $Z_{\text{in}}^e Z_{\text{in}}^o = Z_{0e} Z_{0o} = Z_0^2$, and (7.76) reduces to

$$Z_{\text{in}} = Z_0. \tag{7.78}$$

Thus, as long as (7.77) is satisfied, port 1 (and, by symmetry, all other ports) will be matched.

Now if (7.77) is satisfied, so that $Z_{\text{in}} = Z_0$, we have that $V_1 = V_0$, by voltage division. The voltage at port 3 is

$$V_3 = V_3^e + V_3^o = V_1^e - V_1^o = V_0 \left[\frac{Z_{\text{in}}^e}{Z_{\text{in}}^e + Z_0} - \frac{Z_{\text{in}}^o}{Z_{\text{in}}^o + Z_0} \right], \tag{7.79}$$

where (7.74) has been used. From (7.73) and (7.77), we can show that

$$\frac{Z_{\text{in}}^e}{Z_{\text{in}}^e + Z_0} = \frac{Z_0 + jZ_{0e}\tan\theta}{2Z_0 + j(Z_{0e} + Z_{0o})\tan\theta},$$

$$\frac{Z_{\text{in}}^o}{Z_{\text{in}}^o + Z_0} = \frac{Z_0 + jZ_{0o}\tan\theta}{2Z_0 + j(Z_{0e} + Z_{0o})\tan\theta},$$

so that (7.79) reduces to

$$V_3 = V_0 \frac{j(Z_{0e} - Z_{0o})\tan\theta}{2Z_0 + j(Z_{0e} + Z_{0o})\tan\theta}. \tag{7.80}$$

Now define the coupling coefficient, C, as

$$C = \frac{Z_{0e} - Z_{0o}}{Z_{0e} + Z_{0o}}, \tag{7.81}$$

which we will soon see is actually the midband voltage coupling coefficient, V_3/V_0. Then,

$$\sqrt{1 - C^2} = \frac{2Z_0}{Z_{0e} + Z_{0o}},$$

so that

$$V_3 = V_0 \frac{jC \tan\theta}{\sqrt{1 - C^2} + j \tan\theta}. \tag{7.82}$$

Similarly, we can show that

$$V_4 = V_4^e + V_4^o = V_2^e - V_2^o = 0, \tag{7.83}$$

$$V_2 = V_2^e + V_2^o = V_0 \frac{\sqrt{1 - C^2}}{\sqrt{1 - C^2}\cos\theta + j \sin\theta}. \tag{7.84}$$

Equations (7.82) and (7.84) can be used to plot the coupled and through port voltages versus frequency, as shown in Figure 7.33. At very low frequencies ($\theta \ll \pi/2$), virtually all power is transmitted through port 2, with none being coupled to port 3. For $\theta = \pi/2$, the coupling to port 3 is at its first maximum; this is where the coupler is generally operated, for small size and minimum line loss. Otherwise, the response is periodic, with maxima in V_3 for $\theta = \pi/2, 3\pi/2, \ldots$

For $\theta = \pi/2$, the coupler is $\lambda/4$ long, and (7.82) and (7.84) reduce to

$$\frac{V_3}{V_0} = C, \tag{7.85}$$

$$\frac{V_2}{V_0} = -j\sqrt{1 - C^2}, \tag{7.86}$$

which shows that $C < 1$ is the voltage coupling factor at the design frequency, $\theta = \pi/2$. Note that these results satisfy power conservation since $P_{\text{in}} = (1/2)|V_0|^2/Z_0$, while the output powers are $P_2 = (1/2)|V_2|^2/Z_0 = (1/2)(1-C^2)|V_0|^2/Z_0$, $P_3 = (1/2)|C|^2|V_0|^2/Z_0$, and $P_4 = 0$,so that $P_{\text{in}} = P_2 + P_3 + P_4$. Also observe that there is a 90° phase shift between the two output port voltages; thus this coupler can be used as a quadrature hybrid. In addition, as long as (7.77) is satisfied, the coupler will be matched at the input and have perfect isolation, at any frequency.

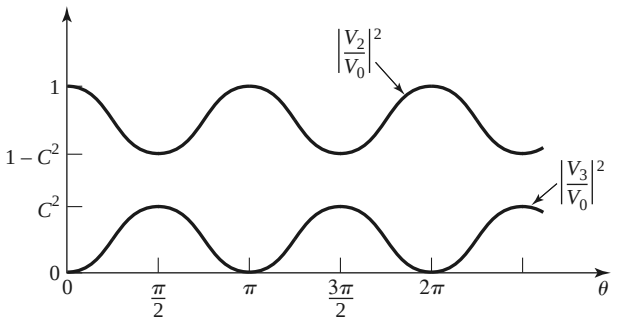

FIGURE 7.33 Coupled and through port voltages (squared) versus frequency for the coupled line coupler of Figure 7.31.

Finally, if the characteristic impedance, Z_0, and the voltage coupling coefficient, C, are specified, then the following design equations for the required even- and odd-mode characteristic impedances can be easily derived from (7.77) and (7.81):

$$Z_{0e} = Z_0\sqrt{\frac{1+C}{1-C}}, \tag{7.87a}$$

$$Z_{0o} = Z_0\sqrt{\frac{1-C}{1+C}}. \tag{7.87b}$$

In the above analysis it was assumed that the even and odd modes of the coupled line structure have the same velocities of propagation, so that the line has the same electrical length for both modes. For coupled microstrip lines, or other non-TEM lines, this condition will generally not be satisfied exactly, and the coupler will have poor directivity. The fact that coupled microstrip lines have unequal even- and odd-mode phase velocities can be intuitively explained by considering the field line plots of Figure 7.28, which show that the even mode has less fringing field in the air region than the odd mode. Thus its effective dielectric constant should be higher, indicating a smaller phase velocity for the even mode. Techniques for compensating coupled microstrip lines to achieve equal even- and odd-mode phase velocities include the use of dielectric overlays and anisotropic substrates.

This type of coupler is best suited for weak coupling, as a large coupling factor requires lines that are too close together to be practical, or a combination of even- and odd-mode characteristic impedances that is nonrealizable.

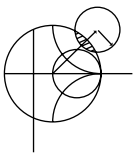

EXAMPLE 7.7 SINGLE-SECTION COUPLER DESIGN AND PERFORMANCE

Design a 20 dB single-section coupled line coupler in stripline with a ground plane spacing of 0.32 cm, a dielectric constant of 2.2, a characteristic impedance of 50 Ω, and a center frequency of 3 GHz. Plot the coupling and directivity from 1 to 5 GHz. Include the effect of losses by assuming a loss tangent of 0.05 for the dielectric material and copper conductors of 2 mil thickness.

Solution

The voltage coupling factor is $C = 10^{-20/20} = 0.1$. From (7.87), the even- and odd-mode characteristic impedances are

$$Z_{0e} = Z_0\sqrt{\frac{1+C}{1-C}} = 55.28\ \Omega,$$

$$Z_{0o} = Z_0\sqrt{\frac{1-C}{1+C}} = 45.23\ \Omega.$$

To use Figure 7.29, we have that

$$\sqrt{\epsilon_r}\,Z_{0e} = 82.0,$$

$$\sqrt{\epsilon_r}\,Z_{0o} = 67.1,$$

and so $W/b = 0.809$ and $S/b = 0.306$. This gives a conductor width of $W = 0.259$ cm and a conductor separation of $S = 0.098$ cm (these values were actually found using a commercial microwave CAD package).

Figure 7.34 shows the resulting coupling and directivity versus frequency, including the effect of dielectric and conductor losses. Losses have the effect of reducing the directivity, which is typically greater than 70 dB in the absence of loss. ■

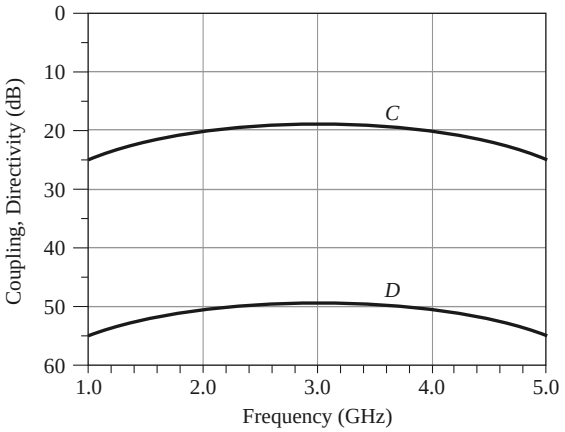

FIGURE 7.34 Coupling versus frequency for the single-section coupler of Example 7.7.

Design of Multisection Coupled Line Couplers

As Figure 7.33 shows, the coupling of a single-section coupled line coupler is limited in bandwidth due to the $\lambda/4$ length requirement. As in the case of matching transformers and waveguide couplers, bandwidth can be increased by using multiple sections. In fact, there is a very close relationship between multisection coupled line couplers and multisection quarter-wave transformers [9].

Because the phase characteristics are usually better, multisection coupled line couplers are generally made with an odd number of sections, as shown in Figure 7.35. Thus, we will assume that N is odd. We will also assume that the coupling is weak ($C \geq 10$ dB), and that each section is $\lambda/4$ long ($\theta = \pi/2$) at the center frequency.

For a single coupled line section, with $C \ll 1$, (7.82) and (7.84) simplify to

$$\frac{V_3}{V_1} = \frac{jC\tan\theta}{\sqrt{1-C^2}+j\tan\theta} \simeq \frac{jC\tan\theta}{1+j\tan\theta} = jC\sin\theta e^{-j\theta}, \tag{7.88a}$$

$$\frac{V_2}{V_1} = \frac{\sqrt{1-C^2}}{\sqrt{1-C^2}\cos\theta + j\sin\theta} \simeq e^{-j\theta}. \tag{7.88b}$$

Then for $\theta = \pi/2$ we have that $V_3/V_1 = C$ and $V_2/V_1 = -j$. The above approximation is equivalent to assuming that no power is lost on the through path from one section to the next, and is similar to the approximation used for the multisection waveguide coupler analysis. It is a good assumption for small C, even though power conservation is violated.

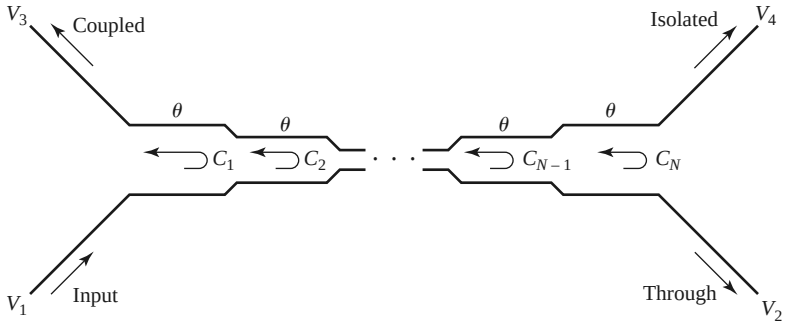

FIGURE 7.35 An N-section coupled line coupler.

Using these results, we can express the total voltage at the coupled port (port 3) of the cascaded coupler in Figure 7.35 as

$$V_3 = \left(jC_1 \sin\theta e^{-j\theta}\right)V_1 + \left(jC_2 \sin\theta e^{-j\theta}\right)V_1 e^{-2j\theta} + \cdots + \left(jC_N \sin\theta e^{-j\theta}\right)V_1 e^{-2j(N-1)\theta}, \tag{7.89}$$

where C_n is the voltage coupling coefficient of the nth section. If we assume that the coupler is symmetric, so that $C_1 = C_N$, $C_2 = C_{N-1}$, etc., we can simplify (7.89) to

$$V_3 = jV_1 \sin\theta e^{-j\theta}\left[C_1\left(1+e^{-2j(N-1)\theta}\right) + C_2\left(e^{-2j\theta} + e^{-2j(N-2)\theta}\right) + \cdots + C_M e^{-j(N-1)\theta}\right]$$

$$= 2jV_1 \sin\theta e^{-jN\theta}\left[C_1 \cos(N-1)\theta + C_2 \cos(N-3)\theta + \cdots + \frac{1}{2}C_M\right], \tag{7.90}$$

where $M = (N+1)/2$.

At the center frequency, we define the voltage coupling factor C_0:

$$C_0 = \left|\frac{V_3}{V_1}\right|_{\theta=\pi/2}. \tag{7.91}$$

Equation (7.90) is in the form of a Fourier series for the coupling as a function of frequency. Thus, we can synthesize a desired coupling response by choosing the coupling coefficients, C_n. Note that in this case we synthesize the coupling response, while in the case of the multihole waveguide coupler we synthesized the directivity response. This is because the path for the uncoupled arm of the multisection coupled line coupler is in the forward direction, and so is less dependent on frequency than the coupled arm path, which is in the reverse direction; this is the opposite situation from the multihole waveguide coupler.

Multisection couplers of this form can achieve decade bandwidths, but coupling levels must be low. Because of the longer electrical length, it is more critical to have equal even- and odd-mode phase velocities than it is for the single-section coupler. This usually means that stripline is the preferred medium for such couplers. Mismatched phase velocities will degrade the coupler directivity, as will junction discontinuities, load mismatches, and fabrication tolerances. A photograph of a coupled line coupler is shown in Figure 7.36.

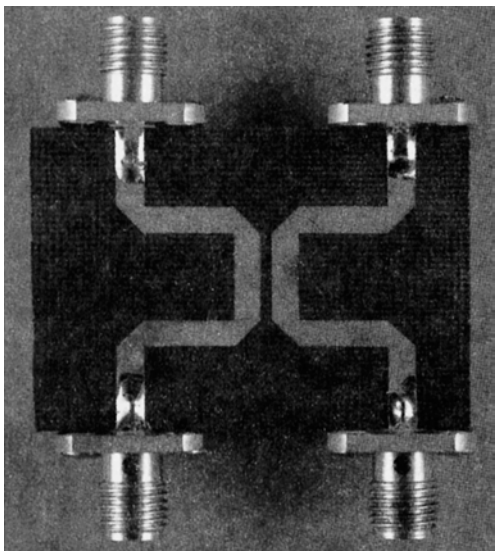

FIGURE 7.36 Photograph of a single-section microstrip coupled line coupler.
Courtesy of M. D. Abouzahra, MIT Lincoln Laboratory, Lexington, Mass.

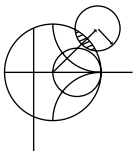

EXAMPLE 7.8 MULTISECTION COUPLER DESIGN AND PERFORMANCE

Design a three-section 20 dB coupled line coupler with a binomial (maximally flat) response, a system impedance of 50 Ω, and a center frequency of 3 GHz. Plot the coupling and directivity from 1 to 5 GHz.

Solution

For a maximally flat response for a three-section ($N = 3$) coupler, we require that

$$\left.\frac{d^n}{d\theta^n}C(\theta)\right|_{\theta=\pi/2} = 0 \quad \text{for } n = 1, 2.$$

From (7.90),

$$\begin{aligned} C = \left|\frac{V_3}{V_1}\right| &= 2\sin\theta\left(C_1\cos 2\theta + \frac{1}{2}C_2\right) \\ &= C_1(\sin 3\theta - \sin\theta) + C_2\sin\theta \\ &= C_1\sin 3\theta + (C_2 - C_1)\sin\theta, \end{aligned}$$

so

$$\begin{aligned} \frac{dC}{d\theta} &= [3C_1\cos 3\theta + (C_2 - C_1)\cos\theta]\Big|_{\pi/2} = 0, \\ \frac{d^2C}{d\theta^2} &= [-9C_1\sin 3\theta - (C_2 - C_1)\sin\theta]\Big|_{\pi/2} = 10C_1 - C_2 = 0. \end{aligned}$$

At midband, $\theta = \pi/2$ and $C_0 = 20$ dB. Thus, $C = 10^{-20/20} = 0.1 = C_2 - 2C_1$. Solving these two equations for C_1 and C_2 gives

$$\begin{aligned} C_1 &= C_3 = 0.0125, \\ C_2 &= 0.125. \end{aligned}$$

From (7.87) the even- and odd-mode characteristic impedances for each section are

$$\begin{aligned} Z_{0e}^1 &= Z_{0e}^3 = 50\sqrt{\frac{1.0125}{0.9875}} = 50.63\ \Omega, \\ Z_{0o}^1 &= Z_{0o}^3 = 50\sqrt{\frac{0.9875}{1.0125}} = 49.38\ \Omega, \\ Z_{0e}^2 &= 50\sqrt{\frac{1.125}{0.875}} = 56.69\ \Omega, \\ Z_{0o}^2 &= 50\sqrt{\frac{0.875}{1.125}} = 44.10\ \Omega. \end{aligned}$$

The coupling and directivity for this coupler are plotted in Figure 7.37. ■

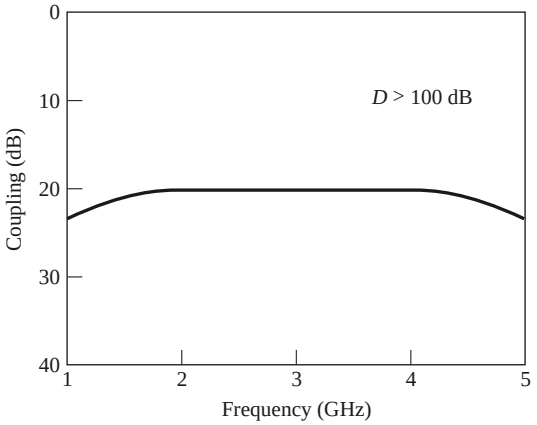

FIGURE 7.37 Coupling versus frequency for the three-section binomial coupler of Example 7.8.

7.7 THE LANGE COUPLER

Generally the coupling in a coupled line coupler is too loose to achieve coupling factors of 3 or 6 dB. One way to increase the coupling between edge-coupled lines is to use several lines parallel to each other, so that the fringing fields at both edges of a line contribute to the coupling. One of the most practical implementations of this idea is the *Lange coupler* [10], shown in Figure 7.38a, where four parallel coupled lines are used with interconnections to provide tight coupling. This coupler can easily achieve 3 dB coupling ratios, with an octave or more bandwidth. The design tends to compensate for unequal even- and odd-mode phase velocities, which also improves the bandwidth. There is a 90° phase difference between the output lines (ports 2 and 3), so the Lange coupler is a type of quadrature hybrid. The main disadvantage of the Lange coupler is probably practical, as the lines are very narrow and close together, and the required bonding wires across the lines increases complexity. This type of coupled line geometry is also referred to as *interdigitated*; such structures can also be used for filter circuits.

The *unfolded* Lange coupler [11], shown in Figure 7.38b, operates in essentially the same way as the original Lange coupler but is easier to model with an equivalent circuit. Such an equivalent circuit consists of a four-wire coupled line structure, as shown in Figure 7.39a. All of the lines have the same width and spacing. If we make the reasonable assumption that each line couples only to its nearest neighbor, and ignore more-distant couplings, then we effectively have a two-wire coupled line circuit, as shown in Figure 7.39b. Then, if we can derive the even- and odd-mode characteristic impedances, Z_{e4} and Z_{o4}, of the four-wire circuit of Figure 7.39a in terms of Z_{0e} and Z_{0o}, the even- and odd-mode characteristic impedances of any adjacent pair of lines, we can apply the coupled line coupler results of Section 7.6 to analyze the Lange coupler.

Figure 7.40a shows the effective capacitances between the conductors of the four-wire coupled line of Figure 7.39a. Unlike the two-line case of Section 7.6, the capacitances of the four lines to ground are different depending on whether the line is on the outside (1 and 4), or on the inside (2 and 3). An approximate relation between these capacitances is [12]

$$C_{\text{in}} = C_{\text{ex}} - \frac{C_{\text{ex}}C_m}{C_{\text{ex}} + C_m}. \tag{7.92}$$

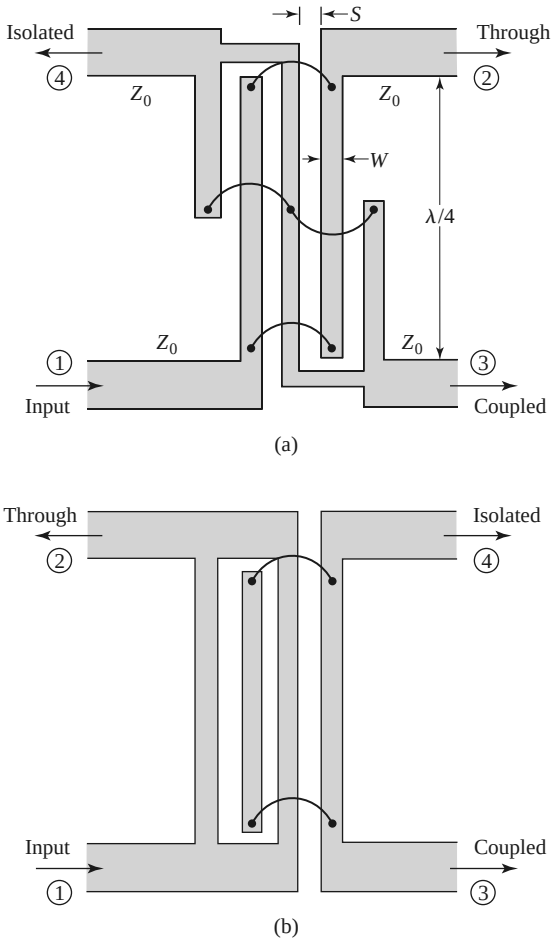

FIGURE 7.38 The Lange coupler. (a) Layout in microstrip form. (b) The unfolded Lange coupler.

For an even-mode excitation, all four conductors in Figure 7.40a are at the same potential, so C_m, has no effect, and the total capacitance of any line to ground is

$$C_{e4} = C_{\text{ex}} + C_{\text{in}}. \tag{7.93a}$$

For an odd-mode excitation, electric walls effectively exist through the middle of each C_m, so the capacitance of any line to ground is

$$C_{o4} = C_{\text{ex}} + C_{\text{in}} + 6C_m. \tag{7.93b}$$

The even- and odd-mode characteristic impedances are then

$$Z_{e4} = \frac{1}{v_p C_{e4}}, \tag{7.94a}$$

$$Z_{o4} = \frac{1}{v_p C_{o4}}, \tag{7.94b}$$

where v_p is the phase velocity of propagation on the line.

Now consider any isolated pair of adjacent conductors in the four-line model; the effective capacitances are as shown in Figure 7.40b. The even- and odd-mode capacitances

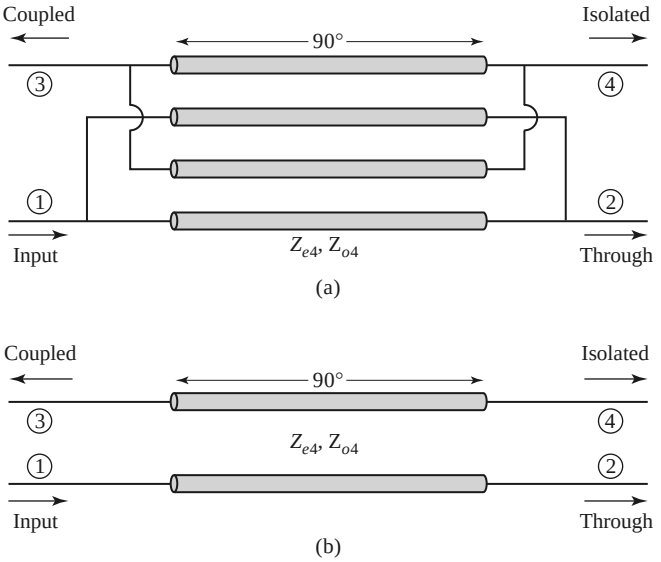

FIGURE 7.39 Equivalent circuits for the unfolded Lange coupler. (a) Four-wire coupled line model. (b) Approximate two-wire coupled line model.

are

$$C_e = C_{\text{ex}}, \tag{7.95a}$$

$$C_o = C_{\text{ex}} + 2C_m. \tag{7.95b}$$

Solving (7.95) for C_{ex} and C_m, and substituting into (7.93) with the aid of (7.92) gives the even-odd mode capacitances of the four-wire line in terms of a two-wire coupled line:

$$C_{e4} = \frac{C_e(3C_e + C_o)}{C_e + C_o}, \tag{7.96a}$$

$$C_{o4} = \frac{C_o(3C_o + C_e)}{C_e + C_o}. \tag{7.96b}$$

Because characteristic impedances are related to capacitance as $Z_0 = 1/v_p C$, we can rewrite (7.96) to give the even/odd mode characteristic impedances of the Lange coupler in terms of the characteristic impedances of a two-conductor line that is identical to any pair

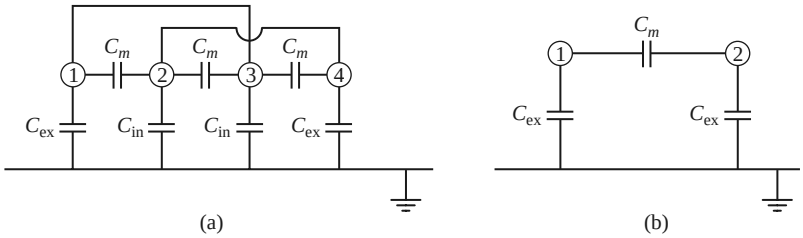

FIGURE 7.40 Effective capacitance networks for the unfolded Lange coupler equivalent circuits of Figure 7.39. (a) Effective capacitance network for the four-wire model. (b) Effective capacitance network for the two-wire model.

of adjacent lines in the coupler:

$$Z_{e4} = \frac{Z_{0o} + Z_{0e}}{3Z_{0o} + Z_{0e}} Z_{0e}, \tag{7.97a}$$

$$Z_{o4} = \frac{Z_{0o} + Z_{0e}}{3Z_{0e} + Z_{0o}} Z_{0o}, \tag{7.97b}$$

where Z_{0e} and Z_{0o} are the even- and odd-mode characteristic impedances of the two-conductor pair.

Now we can apply the results of Section 7.6 to the coupler of Figure 7.39b. From (7.77) the characteristic impedance is

$$Z_0 = \sqrt{Z_{e4} Z_{o4}} = \sqrt{\frac{Z_{0e} Z_{0o} (Z_{0o} + Z_{0e})^2}{(3Z_{0o} + Z_{0e})(3Z_{0e} + Z_{0o})}}, \tag{7.98}$$

and the voltage coupling coefficient is, from (7.81),

$$C = \frac{Z_{e4} - Z_{o4}}{Z_{e4} + Z_{o4}} = \frac{3\left(Z_{0e}^2 - Z_{0o}^2\right)}{3\left(Z_{0e}^2 + Z_{0o}^2\right) + 2Z_{0e} Z_{0o}}, \tag{7.99}$$

where (7.97) was used. For design purposes it is useful to invert these results to give the necessary even- and odd-mode impedances in terms of a desired characteristic impedance and coupling coefficient:

$$Z_{0e} = \frac{4C - 3 + \sqrt{9 - 8C^2}}{2C\sqrt{(1 - C)/(1 + C)}} Z_0, \tag{7.100a}$$

$$Z_{0o} = \frac{4C + 3 - \sqrt{9 - 8C^2}}{2C\sqrt{(1 + C)/(1 - C)}} Z_0. \tag{7.100b}$$

These results are approximate because of the simplifications involved with the application of two-line characteristic impedances to the four-line circuit, and because of the assumption of equal even- and odd-mode phase velocities. In practice, however, these results generally give sufficient accuracy. If necessary, a more complete analysis can be made to directly determine Z_{e4} and Z_{o4} for the four-line circuit, as in reference [13].

7.8 THE 180° HYBRID

The 180° hybrid junction is a four-port network with a 180° phase shift between the two output ports. It can also be operated so that the outputs are in phase. With reference to the 180° hybrid symbol shown in Figure 7.41, a signal applied to port 1 will be evenly split into two in-phase components at ports 2 and 3, and port 4 will be isolated. If the input is applied to port 4, it will be equally split into two components with a 180° phase difference at ports 2 and 3, and port 1 will be isolated. When operated as a combiner, with input signals applied at ports 2 and 3, the sum of the inputs will be formed at port 1, while the

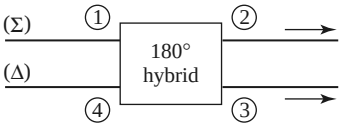

FIGURE 7.41 Symbol for a 180° hybrid junction.

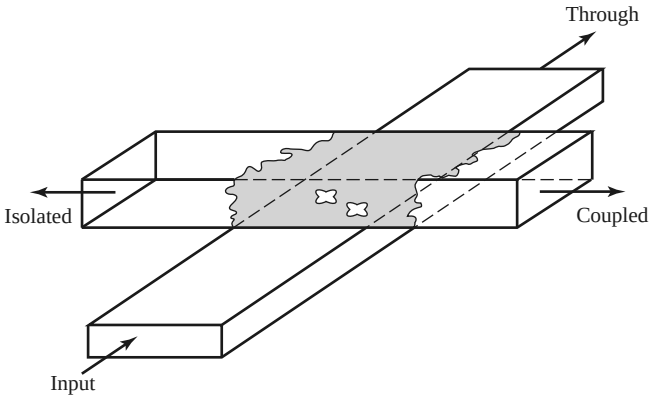

FIGURE 7.51 The Moreno crossed-guide coupler.

7.9 OTHER COUPLERS

Although we have discussed the general properties of couplers and have analyzed and derived design data for several of the most frequently used couplers, there are many other types that we have not treated in detail. In this section we will briefly describe some of these.

Moreno crossed-guide coupler: This is a waveguide directional coupler consisting of two waveguides at right angles, with coupling provided by two apertures in the common broad wall of the guides. See Figure 7.51. By proper design [16], the two wave components excited by these apertures can be made to cancel in the back direction. The apertures usually consist of crossed slots, in order to couple tightly to the fields of both guides.

Schwinger reversed-phase coupler: This waveguide coupler is designed so that the path lengths for the two coupling apertures are the same for the uncoupled port, so that the directivity is essentially independent of frequency. Cancellation in the isolated port is accomplished by placing the slots on opposite sides of the centerline of the waveguide walls, as shown in Figure 7.52, which couple to magnetic dipoles with a 180° phase difference.

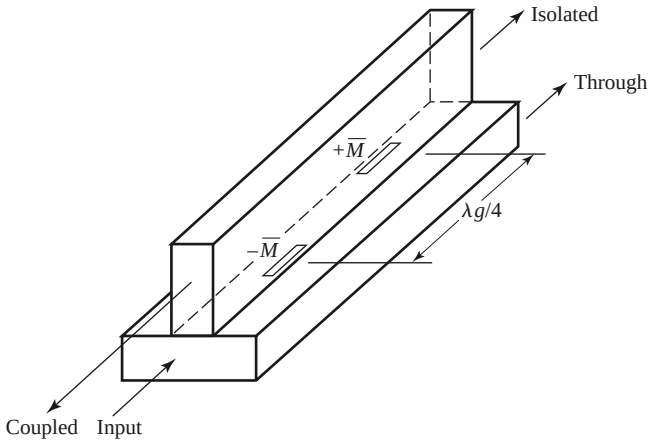

FIGURE 7.52 The Schwinger reversed-phase coupler.

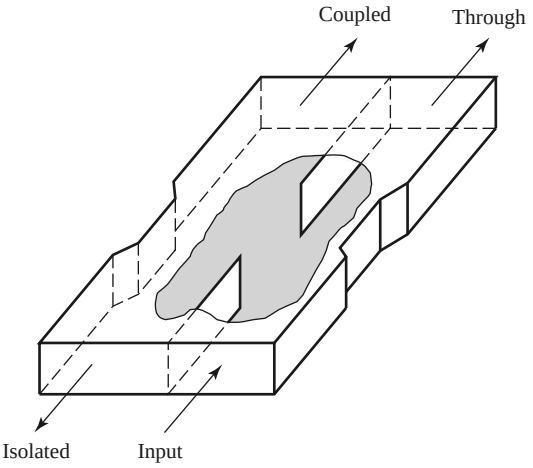

FIGURE 7.53 The Riblet short-slot coupler.

The $\lambda_g/4$ slot spacing leads to in-phase combining at the coupled (backward) port, but this coupling is very frequency sensitive. This is the opposite situation from that of the multihole waveguide coupler discussed in Section 7.4.

Riblet short-slot coupler: This coupler, shown in Figure 7.53, consists of two waveguides with a common sidewall. Coupling takes place in the region where part of the common wall has been removed. In this region both the TE_{10} (even) and the TE_{20} (odd) modes are excited, and by proper design can be made to cause cancellation at the isolated port and addition at the coupled port. The width of the interaction region must be small enough to prevent propagation of the undesired TE_{30} mode. This coupler can usually be made smaller than other waveguide couplers.

Symmetric tapered coupled line coupler: We saw that a continuously tapered transmission line matching transformer was the logical extension of the multisection matching transformer. Similarly, the multisection coupled line coupler can be extended to a continuous taper, yielding a coupled line coupler with good bandwidth characteristics. Such a coupler is shown in Figure 7.54. Generally, both the conductor width and separation can be adjusted to provide a synthesized coupling or directivity response. One way to do this involves the computer optimization of a stepped-section approximation to the continuous taper [17]. This coupler provides a 90° phase shift between the outputs.

Couplers with apertures in planar lines: Many of the above-mentioned waveguide couplers can also be fabricated with planar lines such as microstrip line, stripline, dielectric image lines, or various combinations of these. Some possibilities are illustrated in Figure 7.55.

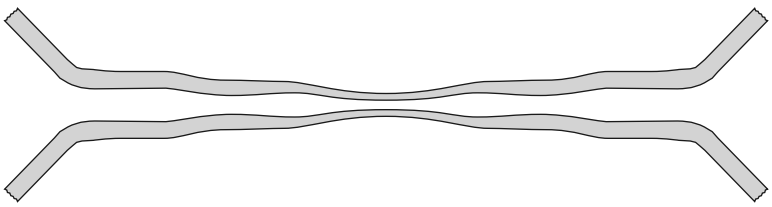

FIGURE 7.54 A symmetric tapered coupled line coupler.

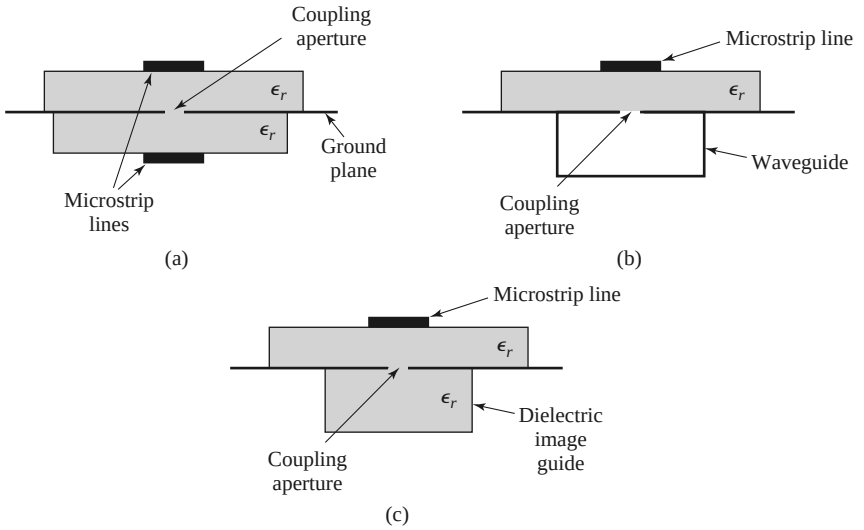

FIGURE 7.55 Various aperture coupled planar line couplers. (a) Microstrip-to-microstrip coupler. (b) Microstrip-to-waveguide coupler. (c) Microstrip-to-dielectric image line coupler.

In principle, the design of such couplers can be carried out using the small-hole coupling theory and analysis techniques used in this chapter. The evaluation of the fields of planar lines, however, is usually much more complicated than for rectangular waveguides.

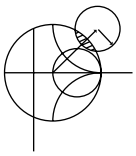

POINT OF INTEREST: The Reflectometer

A *reflectometer* is a circuit that uses a directional coupler to isolate and sample the incident and reflected powers from a load. It is a key component in a scalar or vector network analyzer, as it can be used to measure the reflection coefficient of a one-port network and, in a more general configuration, the scattering parameters of a two-port network. It can also be used as an SWR meter, or as a power monitor in systems applications.

The basic reflectometer circuit shown on the left in the accompanying figure can be used to measure the reflection coefficient magnitude of an unknown load. If we assume a reasonably matched coupler with loose coupling ($C \ll 1$), so that $\sqrt{1-C^2} \simeq 1$, then the circuit can be represented by the signal flow graph shown on the right in the accompanying figure. In operation, the directional coupler provides a sample, V_i, of the incident wave, and a sample, V_r, of the reflected wave. A ratio meter with an appropriately calibrated scale can then measure these voltages and provide a reading in terms of reflection coefficient magnitude, or SWR.

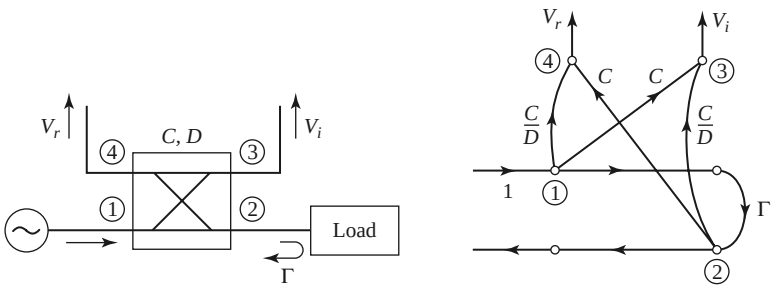

Realistic directional couplers, however, have finite directivity, which means that both incident and reflected powers will contribute to both V_i and V_r, leading to an error. If we assume a unit incident wave from the source, inspection of the signal flow graph leads to the following expressions for V_i and V_r:

$$V_i = C + \frac{C}{D}\Gamma e^{j\theta},$$

$$V_r = \frac{C}{D} + C\Gamma e^{j\phi},$$

where Γ is the reflection coefficient of the load, $D = 10^{(D\,\mathrm{dB}/20)}$ is the numerical directivity of the coupler, and θ, ϕ are the unknown phase delays through the circuit. Then the maximum and minimum values of the magnitude of V_r/V_i can be written as

$$\left|\frac{V_r}{V_i}\right|_{\substack{\max\\ \min}} = \frac{|\Gamma| \pm \dfrac{1}{D}}{1 \mp \dfrac{|\Gamma|}{D}}.$$

For a coupler with infinite directivity this reduces to the desired result of $|\Gamma|$. Otherwise a measurement uncertainty of approximately $\pm 1/D$ is introduced. Good accuracy thus requires a coupler with high directivity, preferably greater than 40 dB.

REFERENCES

[1] A. E. Bailey, ed., *Microwave Measurement*, Peter Peregrinus, London, 1985.

[2] R. E. Collin, *Foundations for Microwave Engineering*, 2nd edition, Wiley–IEEE Press, Hoboken, N.J., 2001.

[3] F. E. Gardiol, *Introduction to Microwaves*, Artech House, Dedham, Mass., 1984.

[4] E. Wilkinson, "An N-Way Hybrid Power Divider," *IRE Transactions on Microwave Theory and Techniques*, vol. MTT-8, pp. 116–118, January 1960.

[5] J. Reed and G. J. Wheeler, "A Method of Analysis of Symmetrical Four-Port Networks," *IRE Transactions on Microwave Theory and Techniques*, vol. MTT-4, pp. 246–252, October 1956.

[6] C. G. Montgomery, R. H. Dicke, and E. M. Purcell, *Principles of Microwave Circuits*, MIT Radiation Laboratory Series, vol. 8, McGraw-Hill, New York, 1948.

[7] H. Howe, *Stripline Circuit Design*, Artech House, Dedham, Mass., 1974.

[8] K. C. Gupta, R. Garg, and I. J. Bahl, *Microstrip Lines and Slot Lines*, Artech House, Dedham, Mass., 1979.

[9] L. Young, "The Analytical Equivalence of the TEM-Mode Directional Couplers and Transmission-Line Stepped Impedance Filters," *Proceedings of the IEEE*, vol. 110, pp. 275–281, February 1963.

[10] J. Lange, "Interdigitated Stripline Quadrature Hybrid," *IEEE Transactions on Microwave Theory and Techniques*, vol. MTT-17, pp. 1150–1151, December 1969.

[11] R. Waugh and D. LaCombe, "Unfolding the Lange Coupler," *IEEE Transactions on Microwave Theory and Techniques*, vol. MTT-20, pp. 777–779, November 1972.

[12] W. P. Ou, "Design Equations for an Interdigitated Directional Coupler," *IEEE Transactions on Microwave Theory and Techniques*, vol. MTT-23, pp. 253–255, February 1973.

[13] D. Paolino, "Design More Accurate Interdigitated Couplers," *Microwaves*, vol. 15, pp. 34–38, May 1976.

[14] J. Hughes and K. Wilson, "High Power Multiple IMPATT Amplifiers," in: *Proceedings of the 4th European Microwave Conference*, Montreux, Switzerland, pp. 118–122, 1974.

[15] R. H. DuHamel and M. E. Armstrong, "The Tapered-Line Magic-T," in: *Abstracts of 15th Annual Symposium of the USAF Antenna Research and Development Program*, Monticello, Ill., October 12–14, 1965.

[16] T. N. Anderson, "Directional Coupler Design Nomograms," *Microwave Journal*, vol. 2, pp. 34–38, May 1959.